



Acceptorless ambient-temperature dehydrogenation and reversible hydrogenation of N-heterocycles over single-atom Co-N-C catalysts

Qingqing Li, Zhiwei Sun, Yilin Wei, Zixu Ma, Liucheng Wang, Renfeng Nie^{*}

National Key Laboratory of Biobased Transportation Fuel Technology, College of Chemical Engineering, Henan Center for Outstanding Overseas Scientists, Zhengzhou University, Zhengzhou 450001, PR China

ARTICLE INFO

Keywords:

Room-temperature dehydrogenation
Atomically dispersed Co-N_x
N-heterocycles
Reversible hydrogen storage
Reaction mechanism

ABSTRACT

Reversible hydrogen storage via Liquid organic hydrogen carriers (LOHCs) is one of the key technologies for efficient utilization of hydrogen energy. How to construct efficient dehydrogenation/hydrogenation catalysts that enable low-temperature catalysis still remains challenging. Herein, we present the design and construction of single-atom Co-N-C(x) catalysts allowing significantly improved acceptorless dehydrogenation of 1,2,3,4-tetrahydroquinoline (THQ). By varying the ligand/Co ratio, the optimal Co-N-C(1.5) can achieve 97.5% dehydrogenated product and 0.82 h⁻¹ TOF value at ambient temperature, overperforming many reported non-noble metal even noble metal catalysts. This catalyst exhibits good recyclability and substrate versatility, enabling ambient temperature dehydrogenation of various N-heterocycles and efficient reverse hydrogenation of aromatic N-heterocycles, thus achieving the loop of reversible hydrogen storage. The active catalyst centers consist of specific Co-N_x moieties and nitrogen species within the carbon support. Controlled experiments reveal that the different performance of Co-N-C(x) is determined by density of the Co-N_x, and the rate-determining step of THQ dehydrogenation is correlated with the bond cleavages in surface-bound THQ. This work offers a promising pathway for energy-efficient and cost-effective hydrogen energy utilization under practical conditions.

1. Introduction

With the rapid depletion of fossil resources and the increasingly prominent environmental issues, hydrogen with a high energy density and zero pollution is being contemplated as the most promising alternative energy. [1] However, hydrogen storage is one of significant challenges for realizing efficient hydrogen utilization. Compared with conventional high pressure storage, chemical storage with liquid organic hydrogen carriers (LOHCs) has enormous advantages in storage efficiency and safety. [2] Among various LOHCs, N-heterocycles attract extensive attention due to their low dehydrogenation barrier and relatively high storage capacity. [3]

The core of chemical hydrogen storage lies in catalyst designing and preparation. Generally, N-heterocycle dehydrogenation can be promoted by metal-free, [4,5] homogeneous [6] and heterogeneous metal catalysts. [7] Metal-free catalysts, like carbon nanotubes, [8] graphene, [9–11] and B/N-doped carbons, [12,13] have found to be active for dehydrogenation originating from rich dopants, but they are difficult to use widely due to the low efficiency and the inevitably harsh reaction conditions. Although homogeneous catalysts (such as Ir, [14–17] Ru,

[18] Fe, [19] Pd, [20,21] Cu, [22,23] and Co [6,24]) exhibit good catalytic efficiency, they suffer from challenges such as separation and recycling. Comparatively, heterogeneous metal catalysts would not only improve the dehydrogenation efficiency but also favor the catalyst recycling. Among them, noble metal catalysts (e.g., Pt, [25–27] Ru, [28, 29] Rh [30,31] and Pd [32–38]) are well-known for their excellent catalytic activity in N-heterocycle dehydrogenation. However, due to the limited resources and high prices, it is imperative to develop inexpensive non-noble metal catalysts from the perspective of economy and industrialization. In this regard, a variety of supported non-noble metal catalysts (e.g., Co, [7,39–42] Ni, [43,44] Fe, [9,45] Mn [46] and Cu [47]) with good dehydrogenation performance were constructed through tuning the metal active sites, [48] metal-support interface structure, [47] and the host-dopant interactions. [49] However, to our best knowledge, most of previous non-noble metal dehydrogenation of N-heterocycles required either high temperature, [50] or excess base [51]/acid [52–55] for C-H activation, or oxidants as hydrogen acceptor, [56] hence resulting in low selectivity, or hydrogen waste. Therefore, the development of an acceptor-free, robust non-noble metal catalyst operating at environmentally benign conditions is highly valuable but

^{*} Corresponding author.

E-mail address: rmie@zzu.edu.cn (R. Nie).

<https://doi.org/10.1016/j.apcatb.2024.123959>

Received 7 December 2023; Received in revised form 6 March 2024; Accepted 14 March 2024

Available online 15 March 2024

0926-3373/© 2024 Elsevier B.V. All rights reserved.

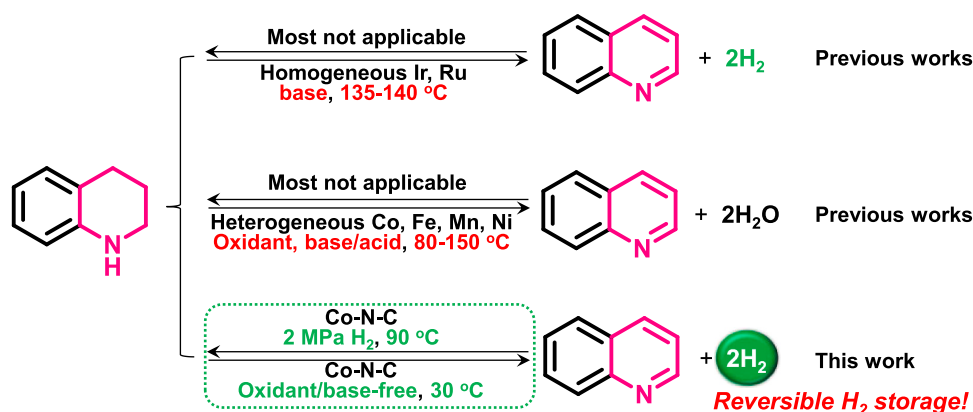


Fig. 1. Schematic representation of the reported strategies [7,45,54,57–59] and our approach for catalytic dehydrogenation to release hydrogen.

challenging.

Single-atom catalysts have advantages such as clear active centers, high metal utilization and adjustable catalytic performance, which are therefore widely used in energy, environmental and catalytic fields. [60–62] Among them, N-doped carbon based single-atom catalysts were widely investigated due to the following features: 1) Nitrogen dopant strengthens the interaction between the carrier and single-atom sites, thereby controlling the electronic and geometric structure, as well as the adsorption orientation and strength towards N-heterocycles; [52] 2) N-doped carbons have shown that activity in dehydrogenation primarily originates from the nitrogen assemblies, which can act as the second active site for further promoting the target reaction. [63] Based on the above analysis, we report porous nitrogen-doped carbon-supported highly dispersed cobalt catalyst (Co-N-C(x)) for acceptorless dehydrogenation of hydroquinolines, hydroisoquinolines, or indolines to the corresponding aromatic N-heterocycles at ambient temperature (Fig. 1). By adjusting the ligand/metal ratio, the metal microstructure as well as activity of the catalyst could be controlled. This catalyst is also versatile for the hydrogenation of aromatic N-heterocycles to the corresponding saturated species as the means to close the loop of reversible hydrogen storage. Wide characterizations and kinetic studies were performed to explore the main active center of Co-N-C(x) and its catalytic mechanism. Moreover, the catalyst recycling and substrate tolerance were investigated. Finally, the reaction process and mechanism were also proposed. The findings in this work pave the way for the design and development of robust non-noble metal dehydrogenation catalysts, critical for reversible hydrogen storage.

2. Experimental section

2.1. Experimental materials

1,10-Phenanthroline (phen, 97%), cobalt acetate (98%), Zinc acetate dihydrate (98%), 1,2,3,4-tetrahydroquinoline (THQ, 97%), 1-acetyl-1,2,3,4-tetrahydroquinoline (98%), 6-methyl-1,2,3,4-tetrahydroquinoline (97%), 2-methyl-1,2,3,4-tetrahydroquinoline (98%), 7-nitro-1,2,3,4-tetrahydroquinoline (97%), 6-hydroxy-tetrahydroisoquinoline (96%), 2-methyl-indoline (99%), indoline (99%), 6-fluoro-1,2,3,4-tetrahydroquinoline (97%), 6-bromo-1,2,3,4-tetrahydroquinoline (97%), 6-chloro-1,2,3,4-tetrahydroquinoline (97%), 6-1,2,3,4-tetrahydroquinoline carboxylic acid (97%), quinoline (98%), isoquinoline (97%), 6-quinolinecarboxylic acid (97%), 6-methoxy-1,2,3,4-tetrahydroquinoline (96%), 2-methyl-indole (97%), indole (98%), 6-methyl-quinoline (97%), 2-methyl-quinoline (98%), 8-methyl-quinoline (98%), 6-methoxy-quinoline (96%), 8-bromo-quinoline (97%), 6-hydroxy-quinoline (96%), 6-hydroxy-isoquinoline (96%), naphthalene (AR) were purchased from Shanghai Macklin Biochemical Technology Co., Ltd. Tetrahydroisoquinoline (isoTHQ, 98%), indole (99%), 6-methoxy-

quinoline (96%), 8-chloro-quinoline (97%), 1,2,3,4-tetrahydronaphthalene (97%) were purchased from Aladdin Chemical. Methanol (MeOH, 99.5%) and ethanol (EtOH, 99.7%) were obtained from Tianjin Yongda Chemical Reagent Co., Ltd. Hydrochloric acid (AR) and nitric acid (AR) were purchased from Xilong Scientific Co., Ltd. Magnesium oxide (MgO, 98%) was purchased from Tianjin Guangfu Technology Development Co., Ltd. All chemicals used in the reaction were of analytical grade and used without further purification.

2.2. Catalyst preparation

2.2.1. Synthesis of $Mg(OH)_2$

Typically, 1.75 g MgO powder and 70 mL deionized water were added into a Teflon-lined stainless steel autoclave of 100 mL capacity, sealed, and maintained at 160 °C for 24 h. Afterwards, the autoclave was allowed to cool to room temperature. The resulting suspension was filtered, washed by 500 mL deionized water, and dried at 80 °C overnight to obtain the $Mg(OH)_2$ powder.

2.2.2. Synthesis of Co-N-C(x)

Cobalt acetate (1 mmol) and phen (1.5 mmol) were dissolved in 50 mL of ethanol, followed by stirring at room temperature for 30 min. Then, 1.38 g $Mg(OH)_2$ was added and the mixture was stirred at 60 °C for 4 h. Afterwards, the ethanol was removed using a rotary evaporator, the obtained powder was dried at 80 °C for 12 h. The powder was heated in a quartz tube to 700 °C at a rate of 10 °C min⁻¹ in N₂ atmosphere and kept at this temperature for 2 h. The obtained black powder (1.06 g) was treated with 1 mol L⁻¹ HCl to remove the MgO, filtered, washed by 500 mL deionized water, and dried at 80 °C under vacuum overnight to obtain Co-N-C(1.5) (0.2 g). Tuning the amount of phen to 1, 2 and 3 mmol yielded the catalysts named Co-N-C(1), Co-N-C(2) and Co-N-C(3), respectively.

2.2.3. Synthesis of N-C

Zinc acetate (1 mmol) and phen (2 mmol) were dissolved in 50 mL of ethanol, followed by stirring at room temperature for 30 min. Then, 1.38 g $Mg(OH)_2$ was added and the mixture was stirred at 60 °C for 4 h. Afterwards, the ethanol was removed using a rotary evaporator, the obtained powder was dried at 80 °C for 12 h. The powder was heated in a quartz tube to 700 °C at a rate of 10 °C min⁻¹ in N₂ atmosphere and kept at this temperature for 2 h. The obtained black powder (1.1 g) was treated with 8 mol L⁻¹ HNO₃ to remove the Zn, filtered, washed by 500 mL deionized water, dried at 80 °C under vacuum overnight to obtain N-C (0.19 g).

2.2.4. Synthesis of 5% $Mg(OH)_2$ /N-C

100 mg N-C, 3.5 mg MgO and 4 mL deionized water were placed in a reactor, stirred at 160 °C for 9 h, and then cooled to room temperature.

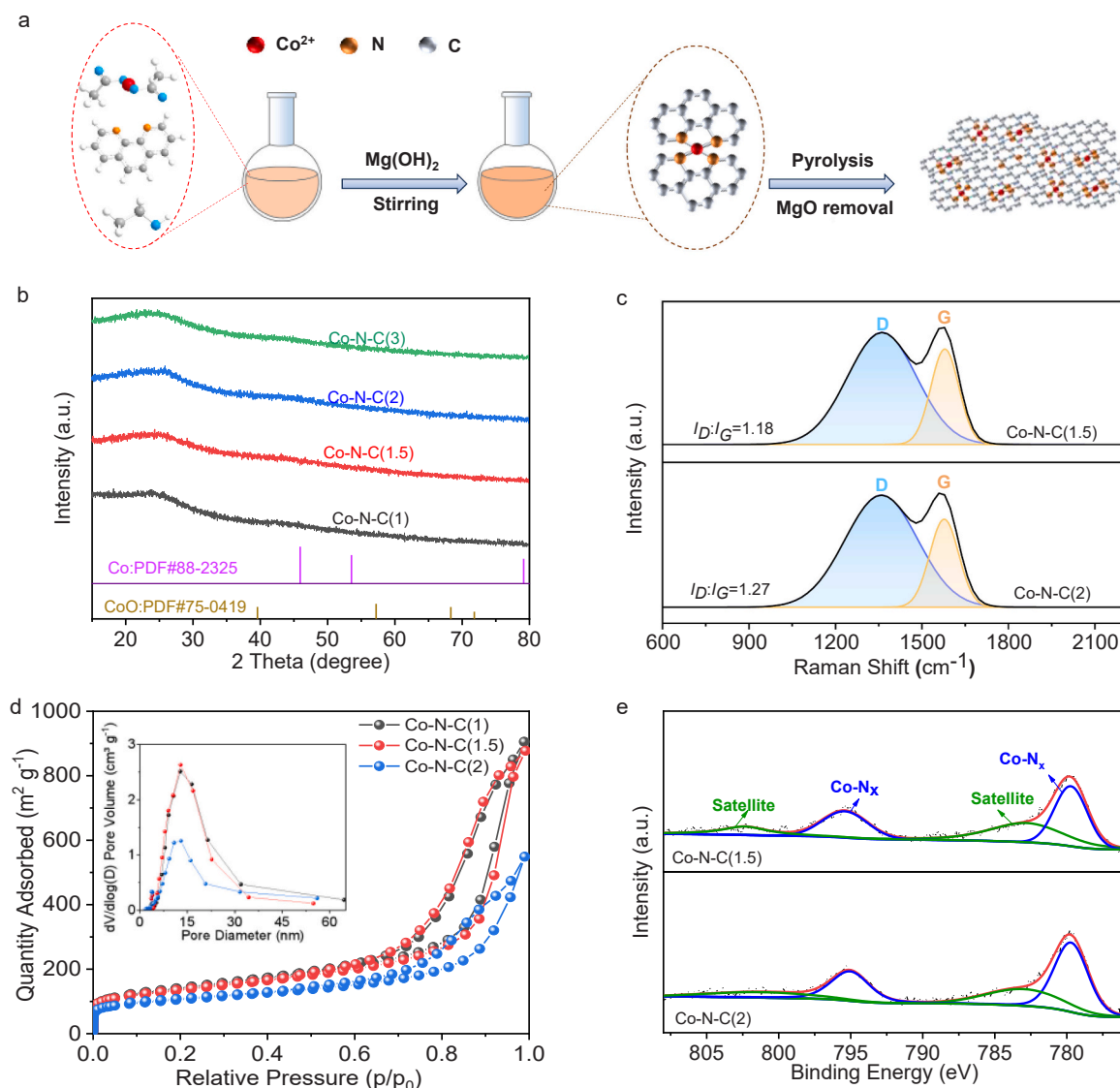


Fig. 2. (a) Schematic of the synthesis process of Co-N-C(x) catalysts, (b) XRD patterns, (c) Raman spectra, (d) N_2 adsorption/desorption isotherms, (e) Co 2p XPS spectra of Co-N-C(x) catalysts.

The suspension was filtered, washed by 500 mL deionized water, and dried at 80 °C to obtain 5% $\text{Mg}(\text{OH})_2/\text{N-C}$ (930 mg).

2.3. Catalyst characterization

The morphology was observed using a high-resolution transmission electron microscope (HRTEM, FEI Talos 200 S), a scanning electron microscope (SEM, ZEISS Sigma 300) and Aberration Corrected High-Angle Annular Dark Field-Scanning Transmission Electron Microscopy (AC HAADF-STEM, Titan Cubed Themis G2300). The crystal structures were determined using X-ray diffraction (XRD) analysis with a Bruker D8 Advance X-ray diffractometer (Bruker, Germany) equipped with $\text{Cu-K}\alpha$ radiation and a scanning range of 15–80°. Raman spectroscopy was conducted using a Renishaw Instruments Ar-ion laser with a wavelength of 514.5 nm to collect spectra in the range of 100–4000 cm^{-1} . The porous structure was characterized using a Micrometrics ASAP 2460 adsorption analyzer after the sample was degassed at 150 °C for 12 h and measured under N_2 adsorption-desorption at −196 °C. The total pore volume was determined by evaporating the N_2 adsorption solution after reaching the relative pressure of 0.99, while the surface area was calculated by the BET method and the pore size was estimated by the

BJH method using the adsorption branch of the isotherm. The metal loading was measured using an Agilent 5110 inductively coupled plasma optical emission spectrometer (ICP-OES). The X-ray photoelectron spectroscopy (XPS) was analyzed using an Escalab 250Xi spectrometer (Thermo Scientific) equipped with an Al $\text{K}\alpha$ X-ray source (1486.6 eV) of 300 W (12 kV/6 mA) with a detection limit of 1%. All binding energies were calibrated using the C 1 s peak at 284.8 eV as a reference.

Hydrogen temperature-programmed desorption (H_2 -TPD) analysis was carried out with a thermal conductivity detector (TCD) on an Auto Chem II 2920. Typically, 0.1 g catalyst was pretreated at 200 °C for 1 h in a helium steam, then the temperature decreased to 50 °C, and 10% H_2/Ar was absorbed for 1 h. Thereafter, a helium flow was introduced as purge gas to remove the unadsorbed H_2 . Finally, desorbed gas signals were recorded at a heating rate of 10 °C min^{-1} to 600 °C.

The temperature-programmed desorption of CO_2 (CO_2 -TPD) was performed using a thermal conductivity detector (TCD) on the Auto Chem II 2920. First, 0.1 g catalyst was pretreated in helium at 200 °C for 1 h, then the temperature was reduced to 50 °C, and CO_2 was absorbed for 1 h. Thereafter, He was introduced as a purge gas to remove unadsorbed CO_2 . After baseline stabilization, gas desorption signals from 50

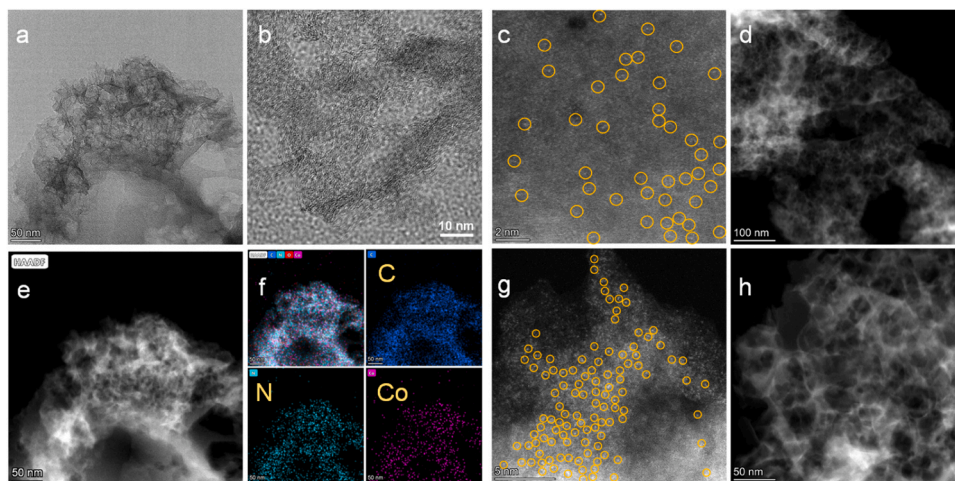


Fig. 3. TEM images of (a-b) Co-N-C(1.5), AC HAADF-STEM images of (c) Co-N-C(1.5) and (g) Co-N-C(2), HAADF-STEM images of (d,e) Co-N-C(1.5) and (h) Co-N-C(2), (f) EDX mapping images of Co-N-C(1.5).

°C to 600 °C were recorded at a warming rate of 10 °C min⁻¹.

The substrate adsorption on catalyst was determined by an ultraviolet spectrophotometer (PElambda750). Initially, a certain amount of THQ or quinoline was dissolved into MeOH and used as the original solution. Then 30 mg catalyst was added into 3 mL original solution and the suspension was stirred at 30 °C. Afterward, 0.1 mL of the reaction mixture was taken at fixed intervals, then diluted and filtered for UV test.

version and yield were further calculated based on a calibration curve established using substrate and product standard solutions with naphthalene as an internal standard for quantification, the formulas are as follows:

$$\text{Conversion (\%)} = \left(1 - \frac{\text{Molar amount of unreacted substrate}}{\text{Initial moles of substrate}} \right) \times 100\%$$

$$\text{Yield (\%)} = \frac{\text{The molar quantity of the product of the reaction}}{\text{Theoretical molar amount of the complete transformation of the substrate}} \times 100\%$$

2.4. Evaluation of catalytic activity

2.4.1. Catalytic dehydrogenation

Dehydrogenation of THQ was carried out a 25-mL glass tube (Fig. S1). In a typical operation, 2 mL of MeOH, 0.1 mmol of THQ, 0.1 mmol of naphthalene, and 20 mg of catalyst were added into the glass tube and the reaction was carried out at room temperature with the protection of 1 bar N₂ (~1 L N₂ balloon) (600 rpm). After the reaction, 0.1 mL of the reaction mixture was taken and diluted with MeOH to 2 mL for analysis. The catalyst was recovered by centrifugation, washed with ethanol (4 × 20 mL), dried overnight in a vacuum at 80 °C, and then treated at 300 °C in H₂ flow for 1 h.

2.4.2. Catalytic hydrogenation

The catalytic hydrogenation of quinoline was carried out in a 50-mL stainless steel high-pressure reactor (Teflon inner). In a typical run, 0.1 mmol of quinoline, 0.1 mmol of naphthalene, 2 mL of MeOH, and 20 mg of catalyst were added into the reactor. Then the reactor was sealed, purged with H₂ for three times, pressurized to 2 MPa, and heated to 90 °C by stirring (600 rpm). After the reaction, the reactor was quenched in cold water to stop the reaction quickly. Then, 0.1 mL of the reaction mixture was taken and diluted with MeOH to 2 mL for analysis.

2.4.3. Product analysis

The supernatant was then taken by centrifugation and analyzed by GC (Fuli GC9790Plus) equipped with a 30 m capillary column (HP-5) and a flame ionization detector (FID). All products were confirmed by using GC-MS (Agilent 5977B MSD) and standard reactants. The con-

$$\text{Turnover frequency (TOF)} = \frac{\text{mole of generated product}}{\text{mole of Metal} \times t(\text{h})}$$

3. Results and discussion

3.1. Catalyst characterization

Co-N-C(x) single-atom catalysts (x=n_{phen}/n_{Co}) were prepared using the support-sacrificial approach (Fig. 2a) by multi-step ultrasonic mixing of Co(OAc)₂, 1,10-phenanthroline (phen) and Mg(OH)₂, followed by pyrolysis under N₂ atmosphere and MgO removal, like an earlier report by Zhang et al. [64] Fig. 2b shows XRD patterns of Co-N-C(x) catalysts. For all catalysts, only a broad diffraction peak at ~25° is observed, corresponding to C(002) diffraction peak. No diffraction peaks for Co species (Co⁰ or CoO_x) are observed, indicating that the Co species in all Co-N-C(x) catalysts exist in highly dispersed state. [50] Moreover, the Co loadings in Co-N-C(1), Co-N-C(1.5), Co-N-C(2) and Co-N-C(3) were measured by inductively coupled plasma mass spectrometry (ICP-MS, Table S1) as 6.75, 5.98, 5.52 and 5.10 wt%, respectively, indicating tuning phen/Co ratio could successfully adjust the Co density in Co-N-C(x) catalysts.

The carbon structure of the Co-N-C(x) was characterized by Raman spectroscopy. As shown in Fig. 2c, all Co-N-C(x) exhibit characteristic carbon peaks at 1358 and 1580 cm⁻¹, corresponding to D and G bands, respectively. Comparatively, Co-N-C(1.5) exhibits a slightly lower I_D/I_G

Table 1

Accepterless THQ dehydrogenation over different catalysts at ambient temperature.^a

Entry	Catalyst	$n_{\text{metal}}/n_{\text{sub}}$	t (h)	Yield (%)	TOF (h^{-1}) ^d
1	none	0	4	0	0
2	Co-N-C(1)	0.23	4	72.6	0.79
3	Co-N-C(1.5)	0.20	4	66.2	0.82
4	Co-N-C(2)	0.19	4	44.9	0.60
5	Co-N-C(3)	0.17	4	36.3	0.52
6 ^b	Co-N-C(1.5)	0.20	12	97.5	0.40
7	Pt/C	0.05	4	26.1	1.27
8	Pd/C	0.09	4	11.7	0.31
9	Ru/C	0.10	4	4.8	0.12
10	N-C	-	4	12.1	-
11	Co(OAc) ₂	1.13	4	1.5	0.003
12	phen	-	4	0.29	-
13 ^c	[Co(phen) ₂](OAc) ₂	0.38	4	0.32	0.002
14	5%Mg(OH) ₂ /N-C	0.86	4	7.02	0.02

^a Reaction conditions: THQ (0.1 mmol), catalyst (20 mg), MeOH (2 mL), 30 °C, 4 h, 1 bar N₂, 600 rpm.

^b 12 h.

^c [Co(phen)₂](OAc)₂ was papered by dissolving cobalt acetate and phen in 2 mL of MeOH ($n_{\text{Co}}/n_{\text{phen}}=1/2$).

^d The TOF values were calculated at 4 h for all entries except entry 6.

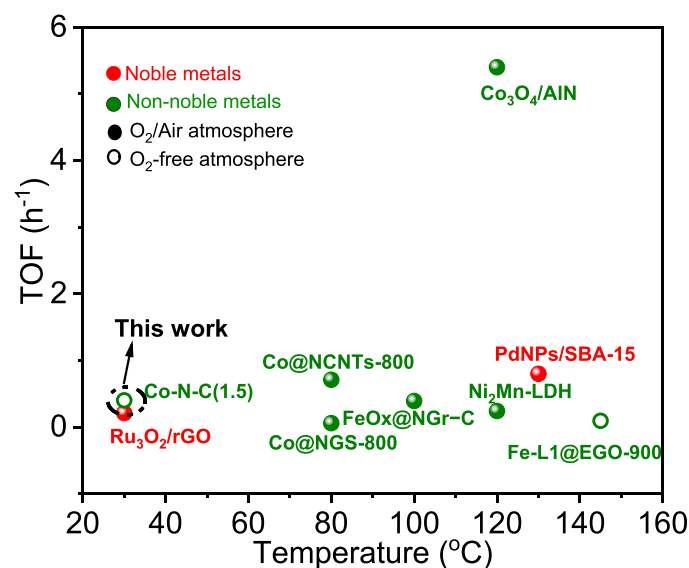


Fig. 4. Comparison of the THQ dehydrogenation of representative noble and non-noble metal catalysts.

value (1.18) than that of Co-N-C(2) ($I_D/I_G = 1.27$), indicating a higher degree of graphitization when adopting a low phen/Co ratio.

Fig. 2d shows the N₂ adsorption-desorption isotherms of the Co-N-C (x). All catalysts exhibit type IV isotherms with an H1 hysteresis loop in relative pressure range of 0.7–1.0 and similar pore size distributions in range of 2–50 nm, indicating the existence of abundant mesopores. As shown in Table S2, the surface areas follow the order: Co-N-C(1) (479 m² g⁻¹) > Co-N-C(1.5) (460 m² g⁻¹) > Co-N-C(2) (353 m² g⁻¹), which are accompanied by similar trend for pore volume: Co-N-C(1) (1.349 cm³ g⁻¹) > Co-N-C(1.5) (1.324 cm³ g⁻¹) > Co-N-C(2) (0.787 cm³ g⁻¹). These results reveal that low phen/Co ratio favors the formation of mesopore owing to relatively abundant template. The high surface area and rich mesopores can effectively reduce mass transfer resistance, thereby facilitating the rapid adsorption and conversion of reactants in following catalytic reactions.

X-ray photoelectron spectroscopy (XPS) was used to analyze the elemental composition and valence state of the catalyst surface. As shown in Fig. S2 and Table S3, C, N, O, and Co coexist in the Co-N-C(x)

Table 2

Accepterless dehydrogenation of various N-heterocycles over Co-N-C(1.5) at ambient temperature.^a

Entry	Substrates	Products	t (h)	Yield (%)
1			12	97.5
2			5	98.4
3			10	99.0
4			10	>99.0
5			0.5	>99.0
6			10	97.5
7			18	97.4
8			24	>99.0
9 ^b			72	98.4
10 ^b			30	90.1
11			48	95.2
12			1.5	97.9
13			1	>99.0

^a Reaction conditions: substrate (0.1 mmol), MeOH (2 mL), Co-N-C(1.5) (20 mg), 30 °C, 1 bar N₂, 600 rpm.

^b 50 °C.

catalysts, and the Co content increases gradually with the increase of the Co/phen ratio, well agreed with the ICP-OES results (Table S1). Co 2p spectra (Fig. 2e) of Co-N-C(1.5) and Co-N-C(2) exhibit that the surface Co mainly exists in form of Co-N_x species. N 1s spectra (Fig. S2) can be fitted into pyridine N (398.24 eV), Co-N_x (399.57 eV), and graphitic N (400.67 eV), and Co-N-C(1.5) contains a higher proportion of Co-N_x than that of Co-N-C(2). These results further prove that increasing Co/phen ratio could achieve higher density of Co-N_x species.

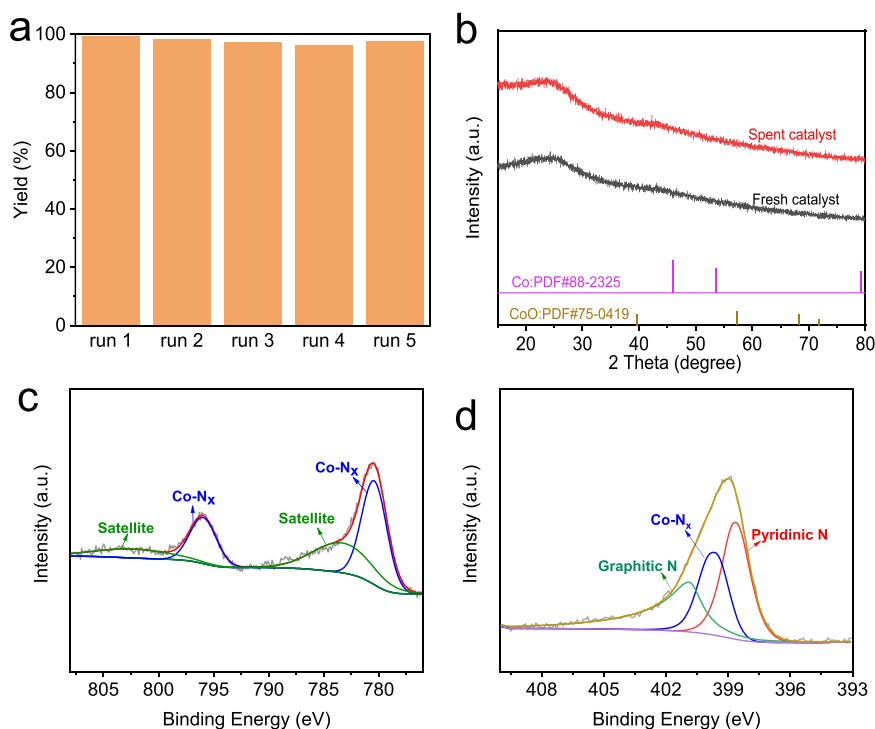


Fig. 5. (a) Durability of Co-N-C(1.5) for THQ dehydrogenation, reaction conditions: substrate (0.3 mmol), MeOH (2 mL), Co-N-C(1.5) (60 mg), 30 °C, 1 bar N₂, 10 h, 600 rpm. (b) XRD patterns, (c) Co 2p XPS spectra (d) N 1s XPS spectra of spent Co-N-C(1.5).

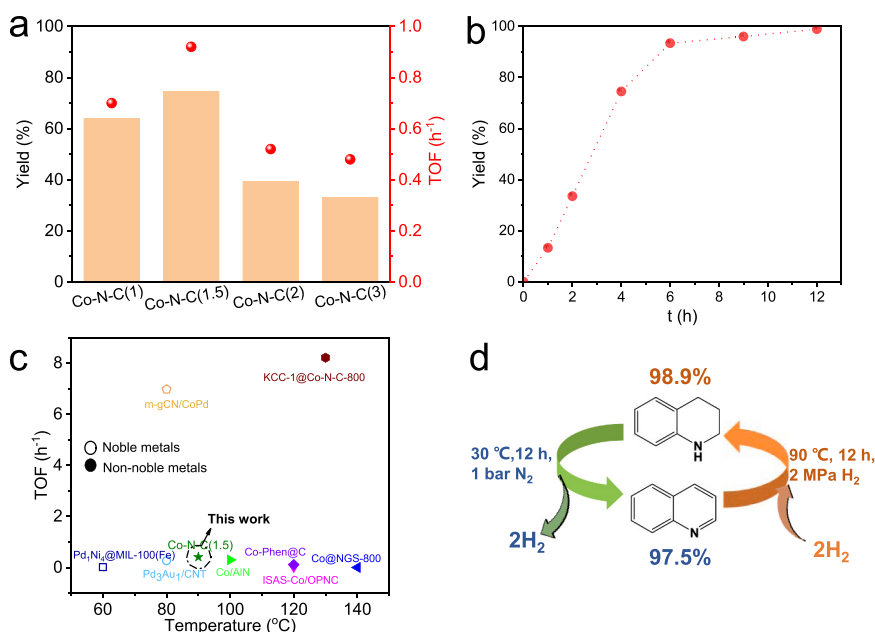
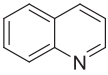
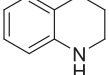
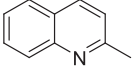
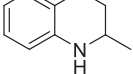
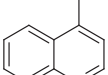
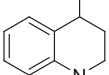
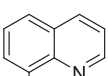
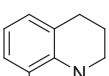
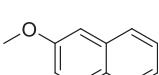
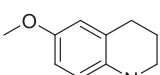
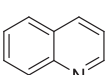
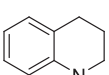
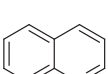
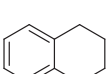
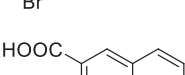
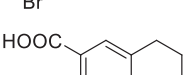
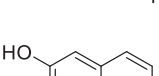
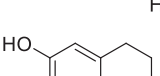
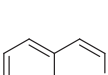
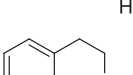
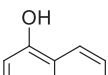
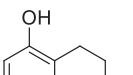


Fig. 6. (a) Selective quinoline hydrogenation with various Co-N-C(x) catalysts. Reaction conditions: quinoline (0.1 mmol), MeOH (2 mL), Co-N-C(x) (20 mg), 90 °C, 2 MPa H₂, 4 h, 600 rpm. (b) Time-activity profiles of quinoline hydrogenation over Co-N-C(1.5). Reaction conditions: quinoline (0.1 mmol), MeOH (2 mL), Co-N-C(1.5) (20 mg), 90 °C, 2 MPa H₂, 600 rpm. (c) Comparison of the quinoline hydrogenation of representative noble and non-noble metal catalysts. (d) Schematic cycle of hydrogen storage via N-heterocycle hydrogenation and dehydrogenation. Reaction conditions: substrate (0.1 mmol), MeOH (2 mL), Co-N-C(1.5) (20 mg), 12h, 600 rpm.

The SEM images (Fig. S3) show that Co-N-C(1.5) and Co-N-C(2) exhibit abundant “honeycomb-like” pore structures, originating from the pore-forming of template. The TEM and HRTEM images (Fig. 3a-b, and S4) indicate that no crystalline or cluster phase of Co are observed in Co-N-C(1.5) and Co-N-C(2), which is further proved by HAADF-STEM images (Fig. 3d, e, h and S4). The AC HAADF-STEM images indicate

that single-atoms of Co are uniformly distributed in both Co-N-C(1.5) and Co-N-C(2) (Figs. 3c and 3g). EDX mapping (Fig. 3f) indicates that C, N and Co are uniformly distributed in the catalyst. These results indicate that Co species are highly dispersed as single-atom form on surface of the porous carbon frameworks and can be coordinated closely with N species.

Table 3The reversible hydrogenation of various N-heterocycles over Co-N-C(1.5). ^a.

Entry	Substrates	Products	t (h)	Yield (%)
1			10	96.4
2			6	98.9
3			12	94.5
4			8	>99.0
5			16.7	96.5
6			6	97.4
7			11	97.5
8			10	>99.0
9 ^b			12	92.6
10 ^b			18	94.5
11 ^b			24	90.0

^a Reaction conditions: substrate (0.1 mmol), MeOH (2 mL), Co-N-C(1.5) (20 mg), 90 °C, 2 MPa H₂, 600 rpm.^b 120 °C.

3.2. Catalytic dehydrogenation of N-heterocycles

Acceptorless THQ dehydrogenation at ambient temperature was chosen as a model reaction to investigate the catalytic activity of various Co-N-C(x) catalysts (Table 1). When no catalyst is added, no dehydrogenated products are detected at 4 h (entry 1). When varying phen/Co ratio from 1 to 3 (entries 2–5), the quinoline yield decreases gradually from 72.6% to 36.3%, respectively, accompanied by > 99% quinoline selectivity for all Co-N-C(x) catalysts. Combined with the Co loadings determined by ICP-OES (Table S1), a volcano relationship is observed between TOF value and Co loading, particularly, the highest TOF value of 0.82 h⁻¹ is achieved over Co-N-C(1.5) (entry 3).

Then, with Co-N-C(1.5) as the optimal catalyst, 97.5% quinoline yield can be achieved when prolonging reaction time to 12 h (entry 6).

Comparatively, Co-N-C(1.5) not only possess a significant advantage in terms of yield but also dehydrogenation selectivity, exhibiting 2.8, 6.2, and 15.1 times higher quinoline yield than those of Pt/C, Pd/C, and Ru/C catalysts, respectively (entries 7–9). In addition, compared with the reported literature (Fig. 4 and Table S4), Co-N-C(1.5) demonstrates a comparable TOF value (0.4 h⁻¹) for acceptorless THQ dehydrogenation at much milder conditions compared to most non-noble metal Co, Ni, Fe-based catalysts (≥80 °C, O₂ atmosphere), and even surpasses the performance of most noble metal catalysts, particularly at high temperatures and in O₂ atmospheres. [30,40,45,50,52,58] These results once again demonstrate the great potential of Co-N-C(1.5) in the mild dehydrogenation of LOHCs.

To investigate the potential applicability of the Co-N-C(1.5) catalyst, acceptorless dehydrogenation of various N-heterocycles was investigated in Table 2. Similar to THQ dehydrogenation at ambient temperature (entry 1), THQ derivatives with electron-donating substituents (-CH₃, -OH, -OCH₃) are also transformed smoothly into the corresponding quinolines with > 98% yield within 0.5–10 h (entries 2–5). F-, Cl- and Br-substituted THQs are also well tolerated to give the corresponding quinolines in > 97.4% yield without dehalogenation (entries 6–8). Although THQ substituted with strong electron-withdrawing groups (7-nitro, 6-carboxy) are converted slowly into the corresponding quinolines, more than 90% yields are achieved at higher temperature or longer reaction time (entries 9–10). Besides, Co-N-C(1.5) was also capable of dehydrogenating isoTHQ, indoline, and substituted indolines to afford the corresponding N-heterocycles in > 95.2% yields (entries 11–13), confirming the broad applicability of the catalyst.

The recyclability of Co-N-C(1.5) catalyst for THQ dehydrogenation was investigated at high (Fig. 5a) and low conversion (Fig. S5). Although a slight increase in activity after the initial run, the spent catalyst appeared stable over the following four cycles (Fig. S5). In comparison to fresh Co-N-C(1.5), XRD patterns (Fig. 5b) and Co 2p XPS spectra (Figs. 5c and 5d) show no significant difference in structure, composition and valence state of the spent catalyst after recycling, revealing the stable Co-N_x structure for dehydrogenation. [4]

3.3. Reversible hydrogenation of N-heterocycles

Catalysts able to complete the cycle of hydrogen capture and release are becoming increasingly attractive. After achieving excellent performance for acceptorless N-heterocycle dehydrogenation over the Co-N-C(x), quinoline hydrogenation was selected for evaluating the performance of the Co-N-C(x) catalysts (Fig. 6a). Similarly, both THQ yield and TOF value follow a volcano relationship as varying the phen/Co ratio, and the Co-N-C(1.5) shows the highest TOF value (0.92 h⁻¹) and THQ yield (77.5%) at 90 °C and 2 MPa H₂. 96% THQ yield could be achieved when prolong reaction time to 9 h (Fig. 6b). Compared to metal catalyst of the literature (Fig. 6c and Table S5), the TOF value of Co-N-C(1.5) is comparable to many noble and non-noble metals, albeit achieved at lower reaction temperatures than most non-noble metals. It should be noted that, the Co-N-C(1.5) catalyst could not only enable the quinoline hydrogenation in the presence of pressurized H₂, but also highly efficient for the ambient-temperature THQ dehydrogenation without hydrogen waste (acceptorless), exhibiting great potential for completing the cycle of hydrogen storage (Fig. 6d).

With Co-N-C(1.5) as optimal catalyst, the substrate scope was extended to a series of other aromatic N-heterocycles (quinolines and indoles) with different functional groups (90 °C, 2 MPa H₂, Table 3). No matter electron-donating or electron-withdrawing groups could provide the desired THQ derivatives with high yield (entries 1–8) without deoxygenation or dechlorination. Moreover, reaction with 7-OH substituted quinoline, isoquinoline and 6-OH substituted isoquinoline achieved > 90% yield when the reaction temperature was raised to 120 °C (entries 9–11), demonstrating the high tolerance of the Co-N-C(1.5) catalyst.

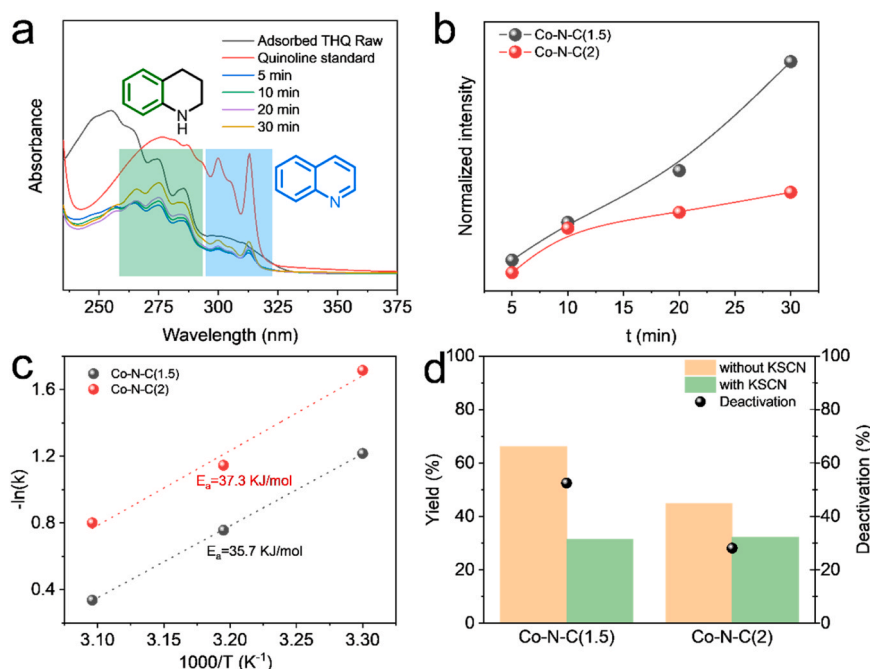


Fig. 7. (a) *In situ* Uv-vis spectra of THQ absorption in presence of Co-N-C(1.5). (b) Data showing the quinoline signal (at 312.7 nm) intensity changes. (c) Calculated Arrhenius plots for Co-N-C(1.5) and Co-N-C(2). (d) Poisoning tests of Co-N-C(1.5) and Co-N-C(2) with KSCN in THQ dehydrogenation. Reaction conditions: THQ (0.1 mmol), MeOH (2 mL), Co-N-C(x) (20 mg), 30 °C, 1 bar N₂, 600 rpm.

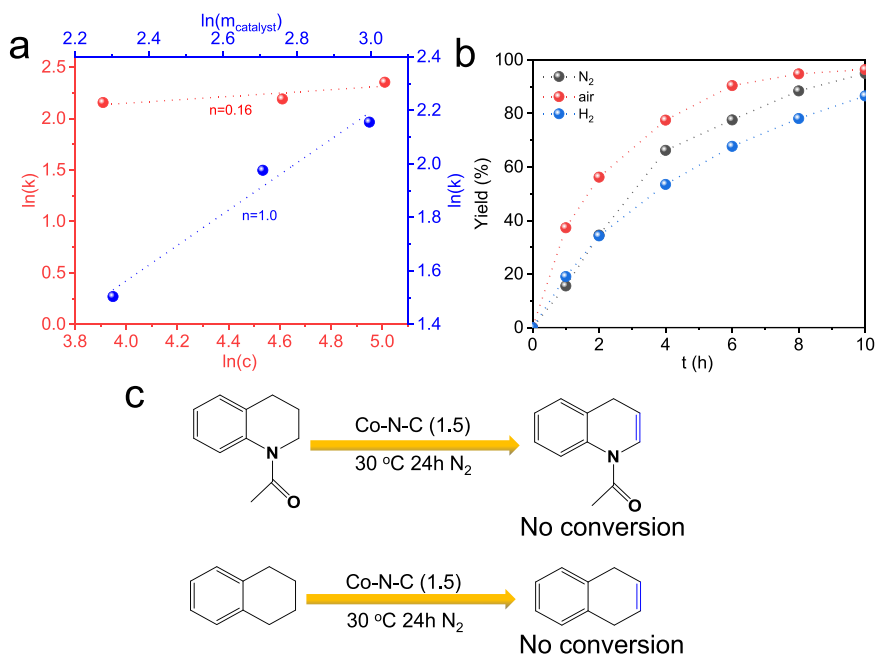


Fig. 8. (a) Measurement of rate orders for Co-N-C(1.5) dosage and THQ concentration at early reaction stage. (b) THQ dehydrogenation with Co-N-C(1.5) under N₂, air and H₂ atmosphere. (c) Control experiments of dehydrogenation over Co-N-C(1.5). Reaction conditions: substrate (0.1 mmol), Co-N-C(1.5) (20 mg), MeOH (2 mL), 30 °C, 24 h, 1 bar N₂, 600 rpm.

3.4. Mechanism investigations

The ambient-temperature activation of THQ over Co-N-C(1.5) and Co-N-C(2) has been first investigated by *in situ* Uv-vis spectra (Fig. 7a and S6). The bands at 265.2, 274.8, and 284.7 nm can be assigned to the absorption signals of aromatic ring of THQ, while the bands at 299.6 and 312.7 nm can be attributed to the absorption signals of conjugate ring of quinoline. [65] After the adsorption of THQ for 5 min, the absorption

bands of quinoline appear and strengthen as prolonging the adsorption time to 30 min, verifying the successful ambient-temperature dehydrogenation of THQ in presence of Co-N-C(1.5). Furthermore, the dependence of quinoline signal intensity (at 312.7 nm) on time in presence of Co-N-C(1.5) and Co-N-C(2) are plotted in Fig. 7b. The rapid increase of the quinoline signal over Co-N-C(1.5) demonstrates that Co-N-C(1.5) is indeed more active than Co-N-C(2) for THQ dehydrogenation at ambient temperature.

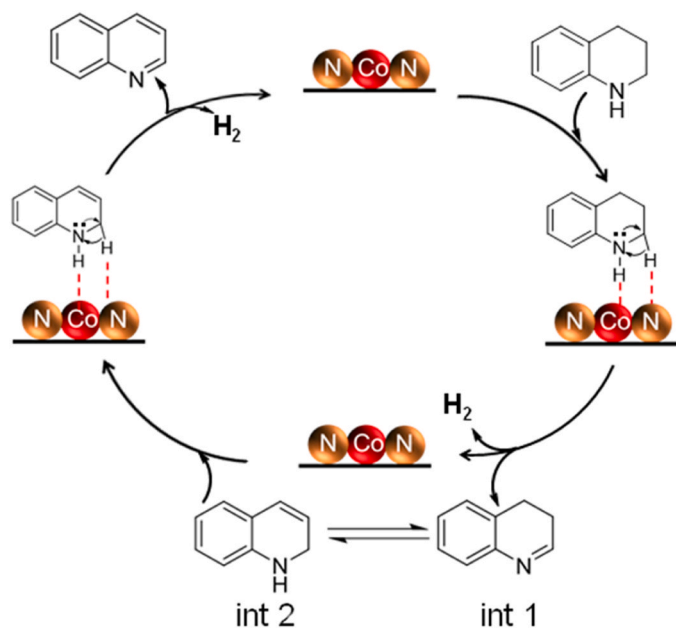


Fig. 9. Proposed reaction mechanism of THQ dehydrogenation over Co-N-C catalyst.

The ability of catalysts to adsorb, dissociate, and rebond hydrogen species can significantly impact dehydrogenation and hydrogenation reactions. [66] Fig. S7 shows the H_2 -TPD curves of Co-N-C(1.5) and Co-N-C(2). After pre-adsorption of H_2 at ambient temperature, the sample was purged with He gas to remove the physically adsorbed H_2 before the desorption ramping was initiated. Compared to Co-N-C(2), a more strengthened desorption signal is observed for Co-N-C(1.5) in range of 50–150 °C, indicating stronger capacity for H-H cleavage or reconstruction. [67]

To discuss the activity of the species for dehydrogenation, the apparent rate constant (k) of Co-N-C(1.5) and Co-N-C(2) were measured (Fig. S8). According to the Arrhenius plot in Fig. 7c, the apparent activation energies (E_a) for Co-N-C(1.5) and Co-N-C(2) are calculated to be 35.7 kJ mol^{-1} and 37.3 kJ mol^{-1} , respectively. The nearly identical apparent activation energies suggest that the active sites of Co-N-C(x) are likely the same. [4] Furthermore, as depicted in CO_2 -TPD profiles (Fig. S9), the variance in basicity does not appear to be the primary factor determining the catalytic differences observed between Co-N-C(1.5) and Co-N-C(2). [68] Control experiments (entries 10–14, Table 1) show that the support itself exhibits certain catalytic activity (12.1% yield). The precursors of Co-N-C(1.5), including $\text{Co}(\text{OAc})_2$, phen and $[\text{Co}(\text{phen})_2](\text{OAc})_2$ are inactive for THQ dehydrogenation. Combined with characterization results and literature, [48] the Co- N_x sites should serve as the main active centers for the dehydrogenation reaction.

To shed light on the role played by the Co- N_x sites, KSCN was used as the binding molecule to join the reaction system for poisoning experiment (Fig. 7d). Although remarkable decrease of the quinoline yield is observed for both Co-N-C(1.5) and Co-N-C(2) after adding KSCN, the nearly similar retained activities for Co-N-C(1.5) (31.4% quinoline yield) and Co-N-C(2) (32.3% quinoline yield) suggest that majority of Co- N_x sites are sensitive to poisoning, while minor Co- N_x sites are inert to KSCN. Therefore, Co-N-C(1.5) should possess higher Co- N_x density (especially for sensitive Co- N_x sites) than that of Co-N-C(2), thus exhibiting better catalytic activity. [48]

To further understand the kinetic information of THQ dehydrogenation over Co-N-C(1.5), the influences of catalyst dosage and THQ concentration were investigated (Fig. 8a, S10). It is found that the apparent rate law had a 0.16 order dependence on THQ and a first order

dependence on the Co-N-C(1.5) catalyst (Fig. 8a). This suggests that there is no internal mass transfer limitation and, more importantly, there is no turnover limitation for THQ adsorption. [4] To study the influence of atmosphere, the THQ dehydrogenation was performed in air or H_2 using Co-N-C(1.5) (Fig. 8b). It is found that the dehydrogenation is slightly promoted by air while restricted by H_2 , suggesting that the recombination of surface H atoms to yield H_2 and its desorption is not rate limiting. [69] Therefore, the reaction mechanism of Co-N-C(1.5) catalyst is different from other oxidative dehydrogenation catalysts, [50] and the rate-determining step is most probably correlated with the bond cleavages in surface-bound THQ. [4]

To further illustrate which bond is firstly activated in THQ dehydrogenation, the control experiment was performed with 1-acetyl-1,2,3,4-tetrahydroquinoline and 1,2,3,4-tetrahydronaphthalene as substrates (Fig. 8c). In either case, there is no N-H bond present, and dehydrogenation product is not detected. These results suggest that the direct dehydrogenation of C-C bond is unfavored, and involvement of the N-H bond may lower the dehydrogenation barrier for THQ. [4] It is reported that 3,4-dihydroquinoline is more stable after the elimination of the first H_2 , implying 1,2-dihydroquinoline can tautomerize to 3, 4-isomer, thus reforming of the N-H bond for next dehydrogenation step.

To confirm the hydrogen production, 10 times scaleup THQ dehydrogenation was conducted in Fig. S11 and Fig. S12. The released gas was collected after 16 h and determined by GC and gas analyser, nearly pure hydrogen was produced with ~90% yield, which is closely with the quinoline yield (~92%). Based on the above control experiments and mechanistic studies, the overall reaction route can be hypothesized as depicted in Fig. 9. THQ is first adsorbed on the Co- N_x surface, followed by sequential activation of the N-H and C-H bonds by the Co and N, respectively, to form intermediate 3,4-dihydroquinoline (int 1). The int 1 will be tautomerized to 1, 2-dihydroquinoline (int 2). After desorption of the first H_2 , a second dehydrogenation step takes place with formation of quinoline and the second H_2 to complete the catalytic cycle.

4. Conclusion

In summary, we present the construction of single-atom Co-N-C(x) catalysts for both the hydrogen releasing *via* ambient-temperature dehydrogenation of N-heterocycles and the reverse hydrogen storage *via* hydrogenation of aromatic N-heterocycles, which are of interest in the context of a hydrogen economy. Detailed investigations show that the catalytic performance can be boosted by varying the phen/Co ratio, and the optimal material exhibit excellent hydrogen production activity reaching up to 0.82 h^{-1} , even exceeding commercial Pd/C, Pt/C and Ru/C catalysts. The Co- N_x species are the main active centers of the Co-N-C(x) and exhibit good recyclability and wide tolerance to N-heterocycles. Mechanism experiments demonstrate that the C/N-H bond breakage of the absorbed THQ is the reaction-determination step. This work provides design ideas for the controlled construction of non-noble metal catalysts that enable low-temperature LOHCs-related hydrogen storage, showing great potential for practical application.

Author contributions

R.N. designed the experiments. R.N. supervised the project. Q.L. performed the experiments. All authors discussed the experiments and results. R.N. and Q.L. prepared and revised the manuscript.

CRediT authorship contribution statement

Qingqing Li: Writing – review & editing, Writing – original draft, Formal analysis, Data curation. **Renfeng Nie:** Writing – review & editing, Writing – original draft, Visualization, Resources, Project administration, Conceptualization. **Yilin Wei:** Visualization, Investigation. **Zhiwei Sun:** Visualization, Investigation. **Liucheng wang:** Project administration. **Zixu Ma:** Visualization, Investigation.

Declaration of Competing Interest

The authors declare no competing financial interest.

Data availability

Data will be made available on request.

Acknowledgements

The authors acknowledge the financial support from the NSFC (U23A20124), the Distinguished Young Researchers' Program of Zhengzhou University in China, Science and Technology Development Plan Joint Fund Project of Henan province (232301420048), Open Funding Project of the State Key Laboratory of Biocatalysis and Enzyme Engineering (SKLBEE20220020) and Program of Processing and Efficient Utilization of Biomass Resources of Henan Center for Outstanding Overseas Scientists (GZS2022007).

Appendix A. Supporting information

Supplementary data associated with this article can be found in the online version at [doi:10.1016/j.apcatb.2024.123959](https://doi.org/10.1016/j.apcatb.2024.123959).

References

- [1] P. Modisha, D. Bessarabov, Aromatic liquid organic hydrogen carriers for hydrogen storage and release, *Curr. Opin. Green. Sustain. Chem.* 42 (2023) 100820, <https://doi.org/10.1016/j.cogsc.2023.100820>.
- [2] S. Lee, T. Kim, G. Han, S. Kang, Y.-S. Yoo, S.-Y. Jeon, J. Bae, Comparative energetic studies on liquid organic hydrogen carrier: A net energy analysis, *Renew. Sustain. Energ. Rev.* 150 (2021) 111447, <https://doi.org/10.1016/j.rser.2021.111447>.
- [3] K.C. Tan, T. He, Y.S. Chua, P. Chen, Recent advances of catalysis in the hydrogenation and dehydrogenation of N-heterocycles for hydrogen storage, *J. Phys. Chem. C* 125 (2021) 18553–18566, <https://doi.org/10.1021/acs.jpcc.1c04783>.
- [4] H. Hu, Y. Nie, Y. Tao, W. Huang, L. Qi, R. Nie, Metal-free carbocatalyst for room temperature acceptorless dehydrogenation of N-heterocycles, *Sci. Adv.* 8 (2022) eabl9478, <https://doi.org/10.1126/sciadv.abl9478>.
- [5] M. Zheng, J. Shi, T. Yuan, X. Wang, Metal-free dehydrogenation of N-heterocycles by ternary h-BCN nanosheets with visible light, *Angew. Chem., Int. Ed.* 57 (2018) 5487–5491, <https://doi.org/10.1002/anie.201800319>.
- [6] R. Xu, S. Chakraborty, H. Yuan, W.D. Jones, Acceptorless, reversible dehydrogenation and hydrogenation of N-heterocycles with a cobalt pincer catalyst, *ACS Catal.* 5 (2015) 6350–6354, <https://doi.org/10.1021/acscatal.5b02002>.
- [7] C. Liao, X. Li, K. Yao, Z. Yuan, Q. Chi, Z. Zhang, Efficient oxidative dehydrogenation of N-heterocycles over nitrogen-doped carbon-supported cobalt nanoparticles, *ACS Sustain. Chem. Eng.* 7 (2019) 13646–13654, <https://doi.org/10.1021/acssuschemeng.8b05563>.
- [8] B. Zheng, J. Xu, J. Song, H. Wu, X. Mei, K. Zhang, W. Han, W. Wu, M. He, B. Han, Nanoparticles and single atoms of cobalt synergistically enabled low-temperature reductive amination of carbonyl compounds, *Chem. Sci.* 13 (2022) 9047–9055, <https://doi.org/10.1039/d2sc01596j>.
- [9] X. Cui, Y. Li, S. Bachmann, M. Scalone, A.-E. Surkus, K. Junge, C. Topf, M. Beller, Synthesis and characterization of iron–nitrogen-doped graphene/core–shell catalysts: efficient oxidative dehydrogenation of N-heterocycles, *J. Am. Chem. Soc.* 137 (2015) 10652–10658, <https://doi.org/10.1021/jacs.5b05674>.
- [10] A. Mollar-Cuni, D. Ventura-Espinosa, S. Martín, H. García, J.A. Mata, Reduced graphene oxides as carbocatalysts in acceptorless dehydrogenation of N-heterocycles, *ACS Catal.* 11 (2021) 14688–14693, <https://doi.org/10.1021/acscatal.1c04649>.
- [11] A. Mollar-Cuni, S. Martín, G. Guisado-Barrios, J.A. Mata, Dual role of graphene as support of ligand-stabilized palladium nanoparticles and carbocatalyst for (de) hydrogenation of N-heterocycles, *Carbon* 206 (2023) 314–324, <https://doi.org/10.1016/j.carbon.2023.02.014>.
- [12] Y. Wang, J. Zhang, X. Wang, M. Antonietti, H. Li, Boron- and fluorine-containing mesoporous carbon nitride polymers: metal-free catalysts for cyclohexane oxidation, *Angew. Chem., Int. Ed.* 49 (2010) 3356–3359, <https://doi.org/10.1002/anie.201000120>.
- [13] L. Shi, D. Wang, A.-H. Lu, A viewpoint on catalytic origin of boron nitride in oxidative dehydrogenation of light alkanes, *Chin. J. Catal.* 39 (2018) 908–913, [https://doi.org/10.1016/s1872-2067\(18\)63060-8](https://doi.org/10.1016/s1872-2067(18)63060-8).
- [14] R. Yamaguchi, C. Ikeda, Y. Takahashi, K.-i. Fujita, Homogeneous catalytic system for reversible dehydrogenation–hydrogenation reactions of nitrogen heterocycles with reversible interconversion of catalytic species, *J. Am. Chem. Soc.* 131 (2009) 8410–8412, <https://doi.org/10.1021/ja9022623>.
- [15] W. Yao, Y. Zhang, X. Jia, Z. Huang, Selective catalytic transfer dehydrogenation of alkanes and heterocycles by an iridium pincer complex, *Angew. Chem., Int. Ed.* 53 (2014) 1390–1394, <https://doi.org/10.1002/anie.201306559>.
- [16] Z. Wang, I. Tonks, J. Belli, C.M. Jensen, Dehydrogenation of N-ethyl perhydrocarbazole catalyzed by PCP pincer iridium complexes: evaluation of a homogenous hydrogen storage system, *J. Organomet. Chem.* 694 (2009) 2854–2857, <https://doi.org/10.1016/j.jorganchem.2009.03.052>.
- [17] K.-i. Fujita, Y. Tanaka, M. Kobayashi, R. Yamaguchi, Homogeneous perdehydrogenation and perhydrogenation of fused bicyclic N-heterocycles catalyzed by iridium complexes bearing a functional bipyridone ligand, *J. Am. Chem. Soc.* 136 (2014) 4829–4832, <https://doi.org/10.1021/ja5001888>.
- [18] S. Muthaiah, S.H. Hong, Acceptorless and base-free dehydrogenation of alcohols and amines using ruthenium-hydride complexes, *Adv. Synth. Catal.* 354 (2012) 3045–3053, <https://doi.org/10.1002/adsc.201200532>.
- [19] S. Chakraborty, W.W. Brennessel, W.D. Jones, A molecular iron catalyst for the acceptorless dehydrogenation and hydrogenation of N-heterocycles, *J. Am. Chem. Soc.* 136 (2014) 8564–8567, <https://doi.org/10.1021/ja504523b>.
- [20] C. Lou, S. Qin, S. Zhang, Z. Lv, A.M. Senan, Z. Chen, G. Yin, Non-redox metal ions promoted oxidative dehydrogenation of saturated C–C bond by simple Pd(OAc)₂ catalyst, *Catal. Commun.* 90 (2017) 5–9, <https://doi.org/10.1016/j.catcom.2016.11.007>.
- [21] Y. Wang, C. Li, J. Huang, External-ligand-free aerobic oxidation of N- and C-containing cyclic systems under Pd-catalyzed conditions, *Asian J. Org. Chem.* 6 (2017) 44–46, <https://doi.org/10.1002/ajoc.201600465>.
- [22] W. Zhou, P. Taboonpong, A.H. Aboo, L. Zhang, J. Jiang, J. Xiao, A convenient procedure for the oxidative dehydrogenation of N-heterocycles catalyzed by FeCl₂/DMSO, *Synlett* 27 (2016) 1806–1809, <https://doi.org/10.1055/s-0035-1561613>.
- [23] D. Jung, M.H. Kim, J. Kim, Cu-Catalyzed aerobic oxidation of Di-tert-butyl hydrazodicarboxylate to Di-tert-butyl azodicarboxylate and its application on dehydrogenation of 1,2,3,4-tetrahydroquinolines under mild conditions, *Org. Lett.* 18 (2016) 6300–6303, <https://doi.org/10.1021/acs.orglett.6b03166>.
- [24] K.-H. He, F.-F. Tan, C.-Z. Zhou, G.-J. Zhou, X.-L. Yang, Y. Li, Acceptorless dehydrogenation of N-heterocycles by merging visible-light photoredox catalysis and cobalt catalysis, *Angew. Chem. Int. Ed.* 56 (2017) 3080–3084, <https://doi.org/10.1002/anie.201612486>.
- [25] Z. Jiang, X. Gong, B. Wang, Z. Wu, T. Fang, A experimental study on the dehydrogenation performance of dodecahydro-N-ethylcarbazole on M/TiO₂ catalysts, *Int. J. Hydrog. Energy* 44 (2019) 2951–2959, <https://doi.org/10.1016/j.ijhydene.2018.11.236>.
- [26] S.K. Moromi, S.M.A.H. Siddiki, K. Kon, T. Toyao, K.-i. Shimizu, Acceptorless dehydrogenation of N-heterocycles by supported Pt catalysts, *Catal. Today* 281 (2017) 507–511, <https://doi.org/10.1016/j.cattod.2016.06.027>.
- [27] Z. Wei, F. Shao, J. Wang, Recent advances in heterogeneous catalytic hydrogenation and dehydrogenation of N-heterocycles, *Chin. J. Catal.* 40 (2019) 980–1002, [https://doi.org/10.1016/s1872-2067\(19\)63336-x](https://doi.org/10.1016/s1872-2067(19)63336-x).
- [28] F. Shao, Z. Yao, Y. Gao, Q. Zhou, Z. Bao, G. Zhuang, X. Zhong, C. Wu, Z. Wei, J. Wang, Geometric and electronic effects on the performance of a bifunctional Ru₂P catalyst in the hydrogenation and acceptorless dehydrogenation of N-heteroarenes, *Chin. J. Catal.* 42 (2021) 1185–1194, [https://doi.org/10.1016/s1872-2067\(20\)63747-0](https://doi.org/10.1016/s1872-2067(20)63747-0).
- [29] X. Nie, Y. Zheng, L. Ji, H. Fu, H. Chen, R. Li, Acceptorless dehydrogenation of amines to nitriles catalyzed by N-heterocyclic carbene–nitrogen–phosphine chelated bimetallic ruthenium (II) complex, *J. Catal.* 391 (2020) 378–385, <https://doi.org/10.1016/j.jcat.2020.09.005>.
- [30] D.V. Jawale, E. Gravel, N. Shah, V. Dauvois, H. Li, I.N.N. Namboothiri, E. Doris, Cooperative dehydrogenation of N-heterocycles using a carbon nanotube–rhodium nanohybrid, *Chem. - Eur. J.* 21 (2015) 7039–7042, <https://doi.org/10.1002/chem.201500148>.
- [31] N.O. Balayeva, Z. Mamiyev, R. Dillert, N. Zheng, D.W. Bahnemann, Rh/TiO₂-Photocatalyzed acceptorless dehydrogenation of N-heterocycles upon visible-light illumination, *ACS Catal.* 10 (2020) 5542–5553, <https://doi.org/10.1021/acscatal.0c00556>.
- [32] J. Oh, T.W. Kim, K. Jeong, J.H. Park, Y.W. Suh, Enhanced activity and stability of a carbon-coated alumina-supported Pd catalyst in the dehydrogenation of a liquid organic hydrogen carrier, perhydro 2-(n-methylbenzyl)pyridine, *ChemCatChem* 10 (2018) 3892–3900, <https://doi.org/10.1002/cctc.201800537>.
- [33] B. Wang, T. Yan, T. Chang, J. Wei, Q. Zhou, S. Yang, T. Fang, Palladium supported on reduced graphene oxide as a high-performance catalyst for the dehydrogenation of dodecahydro-N-ethylcarbazole, *Carbon* 122 (2017) 9–18, <https://doi.org/10.1016/j.carbon.2017.06.021>.
- [34] C. Tang, Z. Feng, X. Bai, In situ preparation of Pd nanoparticles on N-doped graphitized carbon derived from ZIF-67 by nitrogen glow-discharge plasma for the catalytic dehydrogenation of dodecahydro-N-ethylcarbazole, *Fuel* 302 (2021) 121186, <https://doi.org/10.1016/j.fuel.2021.121186>.
- [35] Z. Jiang, X. Gong, S. Guo, Y. Bai, T. Fang, Engineering PdCu and PdNi bimetallic catalysts with adjustable alloying degree for the dehydrogenation reaction of dodecahydro-N-ethylcarbazole, *Int. J. Hydrog. Energy* 46 (2021) 2376–2389, <https://doi.org/10.1016/j.ijhydene.2020.10.123>.
- [36] C. Deraedt, R. Ye, W.T. Ralston, F.D. Toste, G.A. Somorjai, Dendrimer-stabilized metal nanoparticles as efficient catalysts for reversible dehydrogenation/hydrogenation of N-heterocycles, *J. Am. Chem. Soc.* 139 (2017) 18084–18092, <https://doi.org/10.1021/jacs.7b10768>.
- [37] H. Meng, Y. Yang, T. Shen, Z. Yin, J. Zhang, H. Yan, M. Wei, Highly efficient hydrogen production from dehydrogenation reaction of nitrogen heterocycles via

- Pd0-Pd δ + synergistic catalysis, *ACS Catal.* 13 (2023) 9234–9244, <https://doi.org/10.1021/acscatal.3c01522>.
- [38] X. Cui, Z. Huang, A.Pv Muyden, Z. Fei, T. Wang, P.J. Dyson, Acceptorless dehydrogenation and hydrogenation of N- and O-containing compounds on Pd3Au1(111) facets, *Sci. Adv.* 6 (2020) eabb3831, <https://doi.org/10.1126/sciadv.abb3831>.
- [39] A.V. Iosub, S.S. Stahl, Catalytic aerobic dehydrogenation of nitrogen heterocycles using heterogeneous cobalt oxide supported on nitrogen-doped carbon, *Org. Lett.* 17 (2015) 4404–4407, <https://doi.org/10.1021/acs.orglett.5b01790>.
- [40] W. Zhou, D. Chen, Fa Sun, J. Qian, M. He, Q. Chen, Aerobic oxidative dehydrogenation of N-heterocycles catalyzed by cobalt porphyrin, *Tetrahedron Lett.* 59 (2018) 949–953, <https://doi.org/10.1016/j.tetlet.2018.01.094>.
- [41] Y. Han, Z. Wang, R. Xu, W. Zhang, W. Chen, L. Zheng, J. Zhang, J. Luo, K. Wu, Y. Zhu, C. Chen, Q. Peng, Q. Liu, P. Hu, D. Wang, Y. Li, Ordered porous nitrogen-doped carbon matrix with atomically dispersed cobalt sites as an efficient catalyst for dehydrogenation and transfer hydrogenation of N-heterocycles, *Angew. Chem., Int. Ed.* 57 (2018) 11262–11266, <https://doi.org/10.1002/anie.201805467>.
- [42] Y. Hu, X. Li, M. Liu, S. Bartling, H. Lund, J. Rabeah, P.J. Dyson, M. Beller, R. V. Jagadeesh, A cobalt nanocatalyst for the hydrogenation and oxidative dehydrogenation of N-heterocycles, *ChemCatChem* 8 (1) (2023) e202301027, <https://doi.org/10.1002/cctc.202301027>.
- [43] H. Chen, S. He, M. Xu, M. Wei, D.G. Evans, X. Duan, Promoted synergic catalysis between metal Ni and acid-base sites toward oxidant-free dehydrogenation of alcohols, *ACS Catal.* 7 (2017) 2735–2743, <https://doi.org/10.1021/acscatal.6b03494>.
- [44] P. Ryabchuk, A. Agapova, C. Kreyenschulte, H. Lund, H. Junge, K. Junge, M. Beller, Heterogeneous nickel-catalyzed reversible, acceptorless dehydrogenation of N-heterocycles for hydrogen storage, *Chem. Commun.* 55 (2019) 4969–4972, <https://doi.org/10.1039/c9cc00918c>.
- [45] G. Jaiswal, V.G. Landge, D. Jagadeesan, E. Balaraman, Iron-based nanocatalyst for the acceptorless dehydrogenation of N-heterocycles, *Nat. Commun.* 8 (2017) 2147, <https://doi.org/10.1038/s41467-017-01603-3>.
- [46] Z. Zhang, W. Liu, Y. Zhang, J. Bai, J. Liu, Bioinspired atomic manganese site accelerates oxo-dehydrogenation of N-heterocycles over a conjugated Tri-s-triazine framework, *ACS Catal.* 11 (2020) 313–322, <https://doi.org/10.1021/acscatal.0c04651>.
- [47] E. Yuan, P. Ni, J. Xie, P. Jian, X. Hou, Highly efficient dehydrogenation of 2,3-butanediol induced by metal-support interface over Cu-SiO₂ catalysts, *ACS Sustain. Chem. Eng.* 8 (2020) 15716–15731, <https://doi.org/10.1021/acssuschemeng.0c05589>.
- [48] C. Tang, A.E. Surkus, F. Chen, M.M. Pohl, G. Agostini, M. Schneider, H. Junge, M. Beller, A stable nanocobalt catalyst with highly dispersed Co_{Nx} active sites for the selective dehydrogenation of formic acid, *Angew. Chem., Int. Ed.* 56 (2017) 16616–16620, <https://doi.org/10.1002/anie.201710766>.
- [49] M.T. Darby, M. Stamatakis, A. Michaelides, E.C.H. Sykes, Lonely atoms with special gifts: breaking linear scaling relationships in heterogeneous catalysis with single-atom alloys, *J. Phys. Chem. Lett.* 9 (2018) 5636–5646, <https://doi.org/10.1021/acs.jpclett.8b01888>.
- [50] Z.-H. He, Y.-C. Sun, K. Wang, Z.-Y. Wang, P.-P. Guo, C.-S. Jiang, M.-Q. Yao, Z.-H. Li, Z.-T. Liu, Reversible aerobic oxidative dehydrogenation/hydrogenation of N-heterocycles over AlN supported redox cobalt catalysts, *Mol. Catal.* 496 (2020) 111192, <https://doi.org/10.1016/j.mcat.2020.111192>.
- [51] G. Jaiswal, M. Subaramanian, M.K. Sahoo, E. Balaraman, A reusable cobalt catalyst for reversible acceptorless dehydrogenation and hydrogenation of N-heterocycles, *ChemCatChem* 11 (2019) 2449–2457, <https://doi.org/10.1002/cctc.201900367>.
- [52] D. Xu, H. Zhao, Z. Dong, J. Ma, Cobalt nanoparticles apically encapsulated by nitrogen-doped carbon nanotubes for oxidative dehydrogenation and transfer hydrogenation of N-heterocycles, *ChemCatChem* 11 (2019) 5475–5486, <https://doi.org/10.1002/cctc.201901304>.
- [53] D. Xu, H. Zhao, Z. Dong, J. Ma, Catalytically active Co–Nx species stabilized on nitrogen-doped porous carbon for efficient hydrogenation and dehydrogenation of N-heteroarenes, *ChemCatChem* 12 (2020) 4406–4415, <https://doi.org/10.1002/cctc.202000826>.
- [54] J. Li, G. Liu, X. Long, G. Gao, J. Wu, F. Li, Different active sites in a bifunctional Co@N-doped graphene shells based catalyst for the oxidative dehydrogenation and hydrogenation reactions, *J. Catal.* 355 (2017) 53–62, <https://doi.org/10.1016/j.jcat.2017.09.007>.
- [55] J. Wu, J.H. Barnard, Y. Zhang, D. Talwar, C.M. Robertson, J. Xiao, Robust cyclometallated Ir(III) catalysts for the homogeneous hydrogenation of N-heterocycles under mild conditions, *ChemComm* 49 (2013), <https://doi.org/10.1039/c3cc44567d>.
- [56] Z. Dağalan, H. Can, A. Daştan, B. Nişancı, Ö. Metin, Highly efficient hydrogenation and dehydrogenation of N-Heteroarenes catalyzed by mesoporous graphitic carbon nitride supported CoPd alloy nanoparticles, *Tetrahedron* 114 (2022) 132766, <https://doi.org/10.1016/j.tet.2022.132766>.
- [57] M.G. Manas, L.S. Sharninghausen, E. Lin, R.H. Crabtree, Iridium catalyzed reversible dehydrogenation – Hydrogenation of quinoline derivatives under mild conditions, *J. Organomet. Chem.* 792 (2015) 184–189, <https://doi.org/10.1016/j.jorganchem.2015.04.015>.
- [58] W. Zhou, Q. Tao, Fa Sun, X. Cao, J. Qian, J. Xu, M. He, Q. Chen, J. Xiao, Additive-free aerobic oxidative dehydrogenation of N-heterocycles under catalysis by NiMn layered hydroxide compounds, *J. Catal.* 361 (2018) 1–11, <https://doi.org/10.1016/j.jcat.2018.01.030>.
- [59] P. Sánchez, M. Hernández-Juárez, N. Rendón, J. López-Serrano, L.L. Santos, E. Álvarez, M. Paneque, A. Suárez, Hydrogenation/dehydrogenation of N-heterocycles catalyzed by ruthenium complexes based on multimodal proton-responsive CNN(H) pincer ligands, *Dalton Trans.* 49 (2020) 9583–9587, <https://doi.org/10.1039/d0dt02326d>.
- [60] Y. Chen, H. Sun, B.C. Gates, Prototype Atomically Dispersed Supported Metal Catalysts: Iridium and Platinum, *Small* 17 (2021) 2004665, <https://doi.org/10.1002/smll.202004665>.
- [61] W.H. Li, B.C. Ye, J. Yang, Y. Wang, C.J. Yang, Y.M. Pan, H.T. Tang, D. Wang, Y. Li, A single-atom cobalt catalyst for the fluorination of acyl chlorides at parts-per-million catalyst loading, *Angew. Chem., Int. Ed.* 61 (2022) e202209749, <https://doi.org/10.1002/anie.202209749>.
- [62] T. Gan, D. Wang, Atomically dispersed materials: ideal catalysts in atomic era, *Nano Res* 17 (2023) 18–38, <https://doi.org/10.1007/s12274-023-5700-4>.
- [63] Y. Kang, Y. Tang, L. Zhu, B. Jiang, X. Xu, O. Guselnikova, H. Li, T. Asahi, Y. Yamauchi, Porous nanoarchitectures of nonprecious metal borides: from controlled synthesis to heterogeneous catalyst applications, *ACS Catal.* 12 (2022) 14773–14793, <https://doi.org/10.1021/acscatal.2c03480>.
- [64] W. Liu, L. Zhang, W. Yan, X. Liu, X. Yang, S. Miao, W. Wang, A. Wang, T. Zhang, Single-atom dispersed Co–N–C catalyst: structure identification and performance for hydrogenative coupling of nitroarenes, *Chem. Sci.* 7 (2016) 5758–5764, <https://doi.org/10.1039/c6sc02105k>.
- [65] G. Li, H. Yang, H. Zhang, Z. Qi, M. Chen, W. Hu, L. Tian, R. Nie, W. Huang, Encapsulation of nonprecious metal into ordered mesoporous N-doped carbon for efficient quinoline transfer hydrogenation with formic acid, *ACS Catal.* 8 (2018) 8396–8405, <https://doi.org/10.1021/acscatal.8b01404>.
- [66] F. Li, G.-F. Han, H.-J. Noh, J.-P. Jeon, I. Ahmad, S. Chen, C. Yang, Y. Bu, Z. Fu, Y. Lu, J.-B. Baek, Balancing hydrogen adsorption/desorption by orbital modulation for efficient hydrogen evolution catalysis, *Nat. Commun.* 10 (2019) 4060, <https://doi.org/10.1038/s41467-019-12012-z>.
- [67] U. Obenaus, F. Neher, M. Scheibe, M. Dyballa, S. Lang, M. Hunger, Relationships between the hydrogenation and dehydrogenation properties of Rh-, Ir-, Pd-, and Pt-containing zeolites Y studied by in situ MAS NMR spectroscopy and conventional heterogeneous catalysis, *J. Phys. Chem. C* 120 (2016) 2284–2291, <https://doi.org/10.1021/acs.jpcc.5b11367>.
- [68] Y. Zhang, H. Wang, H. Yuan, F. Shi, Hydroxyl group-regulated active nano-Pd/C catalyst generation via in situ reduction of Pd(NH₃)₂Cl₂/C for N-formylation of amines with CO₂/H₂, *ACS Sustain. Chem. Eng.* 5 (2017) 5758–5765, <https://doi.org/10.1021/acssuschemeng.7b00363>.
- [69] Z. Luo, R. Nie, V.T. Nguyen, A. Biswas, R.K. Behera, X. Wu, T. Kobayashi, A. Sadow, B. Wang, W. Huang, L. Qi, Transition metal-like carbocatalyst, *Nat. Commun.* 11 (2020) 4091, <https://doi.org/10.1038/s41467-020-17909-8>.